

Micromagnetic simulation studies of ferromagnetic part-spheres

Richard P. Boardman, Jürgen Zimmermann, and Hans Fangohr
*Computational Engineering and Design Group
School of Engineering Sciences
University of Southampton
United Kingdom*

Alexander A Zhukov and Peter A J de Groot
*School of Physics and Astronomy
University of Southampton
United Kingdom*
(Dated: August 24, 2004)

Novel self-assembly techniques can be used to produce periodic arrays of magnetic nanostructures. We have developed a double template technique using electrochemical deposition. This method produces arrays of dots which are of spherical shape, as opposed to those prepared by standard lithographic techniques, which are usually cylindrical. By varying the amount of material that is deposited electrochemically, spheres of diameter d can be grown up to varying heights $h < d$. Thus different spherical shapes can be created ranging from shallow dots to almost complete spheres.

Using micromagnetic modeling, we calculate numerically the magnetization reversal of soft part spherical particles. The observed reversal mechanisms range from single domain reversal at small radii, to vortex movement in shallow systems at larger radii and vortex core reversal as observed in spheres at larger heights. We present a phase-diagram of the reversal behavior as a function of radius and growth height. Additionally, we compare simulation results of hybrid finite element/boundary element and finite difference calculations for the same systems.

INTRODUCTION

Magnetic recording media created with traditional sputtering methods are nearing fundamental limits as areal bit density increases. Magnetic grains of size orders beneath the paramagnetic limit are unstable at room temperature, making them an ineffective choice for long-term storage media as the many irregular grains used to create a storage bit can no longer be relied on to maintain a particular overall direction of magnetization.

A solution to this problem is to form regular patterned media where data can be stored as one bit per object; the objects in these patterned media can subsequently have a larger size than the grain size in non-patterned media whilst increasing areal density. Photolithographic methods can be used to create these media but are limited to $0.1\mu\text{m}$ sizes. Techniques which use electron beam lithography are not cost-effective on a large scale. Self-assembly methods, however, seem to be an economic way to create nanostructured magnets [1].

Using a chemical self-assembly technique [2] templates can be produced through the evaporation of the liquid from an aqueous suspension of latex spheres of diameter d , leading to the formation of a close packed array. Filling the gaps between the spheres with a non-magnetic material and etching away the latex spheres leaves a honeycomb-like template which can then be filled with a magnetic material up to a height h . Altering the level h to which the honeycomb template is filled allows part-spherical geometries to be produced that range from very shallow, for example height $h = 1/8d$, to almost com-

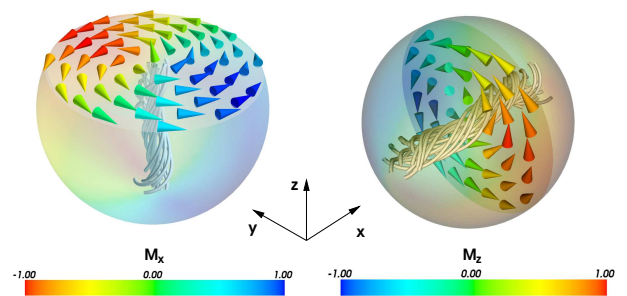


FIG. 1: Remanent magnetization pattern for $d=75\text{nm}$ in (left) a $h = 3/4d$ part sphere and (right) a full sphere where the initial magnetic field was applied in the x direction. The vortex cores are highlighted by streamlines.

pletely full, as $h = 7/8d$.

At the nanometre length scale the magnetic behavior is strongly influenced by the shape of the structure. Related work has been performed on flat cylinders and discs [3–6], spheres [7–9], triangles [10] and other polygons [10, 11]. In this paper, we study the behavior of the new class of part-spherical structures systematically and compute a magnetic reversal phase diagram as a function of diameter and height.

We further compare simulation results obtained with the finite difference method [12] and the hybrid finite element/boundary element method [13].

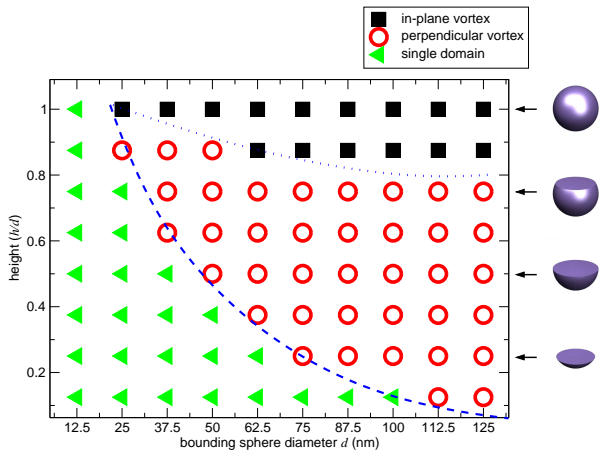


FIG. 2: Phase diagram of reversal mechanisms for $\text{Ni}_{50}\text{Fe}_{50}$ permalloy part-spheres. The dotted and dashed lines are guides to the eye indicating reversal mechanism boundaries.

METHOD

We use the hybrid finite element/boundary element micromagnetic simulation program *magpar* [13] and the finite difference micromagnetic simulation program *OOMMF* [12] to perform the simulations using the material parameters for $\text{Ni}_{50}\text{Fe}_{50}$ permalloy ($J_s = 1.39$ T, $A = 5.85 \times 10^{-12}$ J/m, $K_1 = 0$ J/m³) [14]. These software packages use the Landau-Lifshitz Gilbert equation [15]:

$$\frac{d\mathbf{M}}{dt} = -|\tilde{\gamma}|\mathbf{M} \times \mathbf{H}_{\text{eff}} - \frac{|\tilde{\gamma}|\alpha}{M_s} \mathbf{M} \times (\mathbf{M} \times \mathbf{H}_{\text{eff}}) \quad (1)$$

to compute metastable configurations. We perform simulations on part-spherical geometries where the overall diameter d ranges from 12.5nm to 100nm, and the external magnetic field is applied along the “flat” x direction of the part-sphere.

Starting from an initially uniform magnetization state pointing in the $+x$ direction, we apply a high magnetic field capable of maintaining a nearly homogeneous magnetization and reduce this field in steps of 1mT until the magnetization is reversed.

RESULTS

Figure 2 shows a phase diagram of remanent magnetization states for simulated systems where the height h increases from $1/8d$ to d in $1/8d$ steps and d varies between 12.5nm and 125nm.

We observe three distinct reversal mechanisms. Taking $d=50\text{nm}$, for $h/d \leq 0.375$ the reversal is coherent; all the magnetic moments remain aligned and rotate homogeneously. Between $h/d = 0.5$ and $h/d = 0.875$ an out-of-plane vortex forms with a core perpendicular to

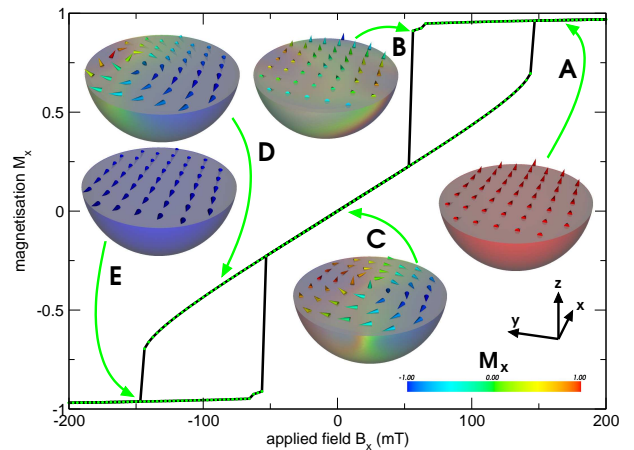


FIG. 3: Reversal mechanism for $d=50\text{nm}$, $h=0.5d$.

the applied field after some initial energy barrier is overcome and this can freely move around the inside of the part-sphere with the applied field. This is similar to the behavior seen in cylindrical particles [4–6, 16]. We will now discuss the reversal mechanism in more detail.

Figure 3 shows the perpendicular vortex reversal behavior. Point A shows the homogeneously aligned state at high applied field, though there is a small C-state-like shift in the x - z direction at the extremities in order to minimise dipolar energy. At point B there is a shift into an S-like state in the x - y direction, where the magnetic moments at the edges of the half-sphere persist in the applied field direction while the moments towards the centre are aligned a few degrees away from the x direction into the y direction. Reducing the field further overcomes an energy barrier and a perpendicular (*i.e.* the core of the vortex points in the z direction) vortex is formed. Point C shows the remanent state of the half-sphere with this vortex in the centre; the net magnetization in the x direction is now zero. Point D shows the effects of a continued field reduction; the vortex has shifted further into the y direction appropriate for allowing the majority of the magnetic moments to point in the negative x direction. Finally, at point E the external field is now sufficiently low to remove the vortex from the system and a homogeneously aligned state remains.

Figure 4 shows the reversal mechanism with an in-plane vortex for a sphere (*i.e.* $h/d = 1.0$). Point A shows a homogeneous alignment of the magnetic moments in the x direction, which persists until point B, where the field has been lowered enough to overcome the energy barrier and allow an in-plane (*i.e.* where the core points in the x direction) vortex to form; this also allows the majority of the magnetization to continue pointing in the x direction. As the field is further reduced, the x component of the magnetization outside the vortex core continues to follow the applied field; however the core remains pointing wholly in the direction of the initial ap-

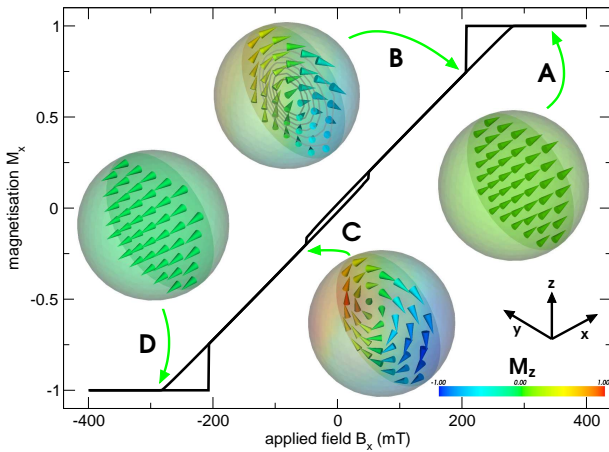


FIG. 4: Reversal mechanism for $d=100\text{nm}$, $h=d$. The centre of the vortex core in inset B and C always remains in the centre of the y - z plane (see also figure 1, right). Inset B shows isolines of M_x in the y - z cutplane to demonstrate this.

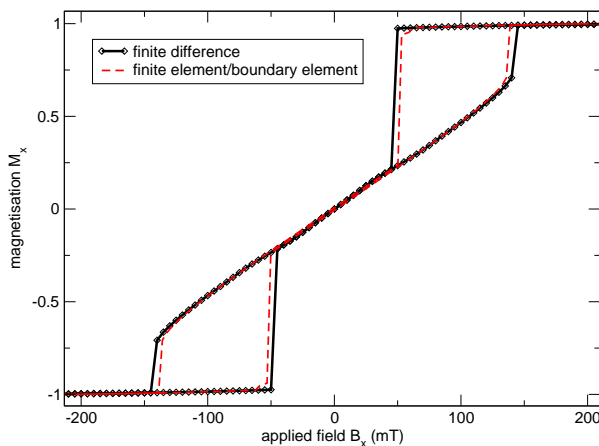


FIG. 5: Hysteresis loops for a $d=50\text{nm}$ half-sphere obtained with (solid line) the finite difference method and (dashed line) the hybrid finite element/boundary element method.

plied field. At point C, after the field is reduced below zero the core of the vortex flips over, responsible for the “minor” hysteresis loop around $B_x = 0$. The vortex can exit the system when the field is further reduced and the magnetization becomes homogeneous (point D).

Our simulation results agree with the computation of the critical radius [17, p305] of single-domain to vortex state transition for $\text{Ni}_{50}\text{Fe}_{50}$ permalloy in spheres of radius 12.4nm ($d=24.8\text{nm}$): a single-domain remanent state is observed in our simulations of spheres of diameter 24nm and below where the exchange energy is dominant, whilst an in-plane vortex is in the remanent state when the diameter is 25nm as the dipolar energy becomes preponderant.

Figure 5 shows results computed during the simulation of a half-sphere of diameter 50nm using two different simulation packages that employ the finite difference

method [12] and the hybrid finite element/boundary element method [13] respectively. There is good agreement between the two packages.

SUMMARY

We have simulated the magnetization reversal in part-spherical particles, and three separate remanent states — single-domain, out-of-plane vortex and in-plane vortex — have been observed.

As the diameter of the part-spherical particle decreases, a larger h/d is necessary for a vortex to form. As h is increased, the magnetization is more likely to form a vortex. Below a critical radius of 12.4nm for $\text{Ni}_{50}\text{Fe}_{50}$, all h/d values will result in a single-domain remanent state.

We have used two different simulation packages and observed good agreement.

- [1] A. A. Zhukov, A. V. Goncharov, P. A. J. de Groot, P.N.Bartlett, and M.A.Ghanem, *J. Appl. Phys.* **93**, 7322 (2003).
- [2] M. A. Ghanem, P. N. Bartlett, P. A. J. de Groot, and A. Zhukov, *Electrochemistry Communications* **6**, 447 (2004).
- [3] R. P. Cowburn, A. O. Adeyeye, and M. E. Welland, *New Journal of Physics* **1**, 16 (1999).
- [4] R. P. Cowburn, D. K. Koltsov, A. O. Adeyeye, M. E. Welland, and D. M. Tricker, *Phys. Rev. Lett.* **83**, 1042 (1999).
- [5] S. P. Li, M. Natali, A. Lebib, A. Péin, Y. Chen, and Y. B. Xu, *J. Magn. Magnetic Materials* **241**, 447 (2002).
- [6] K. Ha, R. Hertel, and J. Kirschner, *Phys. Rev. B* **67**, 064418 (2003).
- [7] J. C. H. Stapper, *J. Appl. Phys.* **40**, 798 (1969).
- [8] I. Eisenstein and A. Aharoni, *J. Appl. Phys.* **47**, 321 (1975).
- [9] J. Lam, *J. Appl. Phys.* **72**, 5792 (1992).
- [10] R. P. Cowburn, *Journal of Physics D* **33**, R1 (2000).
- [11] R. P. Cowburn and M. E. Welland, *Phys. Rev. B* **58**, 9217 (1998).
- [12] M. J. Donahue and D. G. Porter, *OOMMF User's Guide*, National Institute of Standards and Technology, Gaithersburg, MD (1999), interagency Report NISTIR 6376.
- [13] W. Scholz, J. Fidler, T. Schrefl, D. Süß, R. Dittrich, H. Forster, and V. Tsiantos, *Comp. Mater. Sci.* **28**, 366 (2003).
- [14] R. Skomski and J. M. D. Coey, *Permanent Magnetism*, Series in Condensed Matter Physics (Institute of Physics, 1999).
- [15] L. D. Landau and E. M. Lifshitz, *Physikalische Zeitschrift der Sowjetunion* **8**, 153 (1935).
- [16] R. P. Boardman, H. Fangohr, A. V. Goncharov, A. A. Zhukov, P. A. J. de Groot, and S. J. Cox, *J. Appl. Phys.* **95**, 7037 (2004).
- [17] R. C. O'Handley, *Modern Magnetic Materials: Principles and Applications* (John Wiley and Sons, Inc., 1999).